

# Mechanism of Magnesium Transport in Spinel Chalcogenides

Mohsen Sotoudeh, Manuel Dillenz, and Axel Groß\*

Batteries based on multivalent ions such as magnesium have been attracting considerable attention due to their potential for high energy densities, but their low ion mobility remains an obstacle. Herein, ionic conductivity in spinel host materials, which represent a promising class of cathode and solid-electrolyte materials in batteries, is addressed. Based on periodic density functional theory calculations, the important parameters that determine the mobility and insertion of ions are identified. In particular, the critical role that trigonal distortions of the spinel structure play for the ion mobility is highlighted. It is shown that it is the competition between coordination and bond length that governs the Mg site preference in spinel compounds upon trigonal distortions. This can only be understood by also taking covalent interactions into account. This reveals that purely ionic concepts are not sufficient to understand mobility in crystalline battery materials. Furthermore, the calculations suggest that anionic redox plays a much more important role in sulfide and selenide spinels than in oxide spinels. The findings shed light on the fundamental mechanisms underlying ionic conductivity in solid hosts and thus may contribute to improvement of ion transport in battery electrodes.

## 1. Introduction

The development of Li-ion batteries (LIBs) had a major impact on the widespread use of portable electronic devices. However, there are safety and abundance issues associated with LIBs<sup>[1,2]</sup> that motivate the search for alternative battery chemistries.<sup>[3,4]</sup> As a promising alternative, magnesium has been proposed<sup>[5–8]</sup> as an active element with a much higher earth abundance of 13.9% compared to

$7 \times 10^{-4}\%$  of Li. The ionic radii of  $\text{Mg}^{2+}$ , 0.86 Å, and  $\text{Li}^+$ , 0.90 Å, are rather similar,<sup>[1]</sup> but Mg has the advantage of being a bivalent ion, which leads to a higher volumetric capacity of Mg metal anodes compared to Li, 3833 mAh  $\text{cm}^{-3}$  versus 2062 mAh  $\text{cm}^{-3}$ , and also to a low reduction potential of  $-2.37$  V versus the standard hydrogen electrode (SHE) compared to  $-3.05$  V of Li.<sup>[9,10]</sup> Furthermore, Mg-ion batteries (MIBs) exhibit a low tendency for dendrite formation<sup>[11–15]</sup> and a high melting point.

A high multivalent ionic conductivity of 1–10 mS  $\text{cm}^{-1}$  has been achieved in MIBs at high temperatures.<sup>[16,17]</sup> However, a major problem for MIBs lies in the sluggish kinetics during intercalation at room temperature.<sup>[2,18]</sup> It should be noted that the design of chemically stable electrodes with high ionic conductivity is highly desirable,<sup>[2,19–23]</sup> as a low ionic mobility can severely limit the performance of batteries.


To address the slow migration of Mg ions in cathode materials at low temperatures,

Chevreil phases and layered and spinel  $\text{TiS}_2$  structures have been studied in detail.<sup>[24]</sup> A Mg-ion migration barrier of about 550 meV was found in cubic  $\text{Ti}_2\text{S}_4$  using galvanostatic intermittent titration technique measurements. Note that typically maximum migration barriers of  $\approx 525$  meV for micron-sized particles and  $\approx 650$  meV for nanosized particles are assumed to be compatible with an adequate battery operation.<sup>[25]</sup> Studies on the sulfide and selenide spinel frameworks indicate low-energy barriers for Mg-ion diffusion comparable to those of LIBs.<sup>[26]</sup> In contrast, oxide spinel cathode materials exhibit high migration barriers for Mg ions, which are caused by the relatively strong Coulombic attraction between the guest  $\text{Mg}^{2+}$  and host oxygen lattice,<sup>[23]</sup> which leads to a lower ion mobility. The smaller electronegativity of sulfur and selenium lattices enlarges the lattice constant of these materials and thus also their ion mobility as typically diffusion barriers become smaller for larger lattice constants. Nevertheless, the increase of the ion mobility through the lowering of diffusion barriers is also accompanied by lower Mg insertion energies into the spinel structures, which lowers the voltage<sup>[27,28]</sup> and thus causes a reduction of the energy densities of chalcogenide materials.

Recently,  $\text{MgSc}_2\text{Se}_4$  has been found to be a super ionic conductor exhibiting a high Mg-ion conductivity of 0.1 mS  $\text{cm}^{-1}$  at room temperature.<sup>[26]</sup> This high ion mobility not only makes  $\text{MgSc}_2\text{Se}_4$  a promising cathode material for MIBs, but also suggests that it could be used as a solid electrolyte. However, solid

M. Sotoudeh, M. Dillenz, A. Groß  
Institute of Theoretical Chemistry  
Ulm University  
Albert-Einstein-Allee 11, Ulm 89081, Germany  
E-mail: axel.gross@uni-ulm.de

A. Groß  
Electrochemical Energy Storage  
Helmholtz Institute Ulm (HIU)  
Helmholtzstraße 11, Ulm 89069, Germany

 The ORCID identification number(s) for the author(s) of this article can be found under <https://doi.org/10.1002/aesr.202100113>.

© 2021 The Authors. Advanced Energy and Sustainability Research published by Wiley-VCH GmbH. This is an open access article under the terms of the Creative Commons Attribution License, which permits use, distribution and reproduction in any medium, provided the original work is properly cited.

DOI: 10.1002/aesr.202100113

electrolytes need to exhibit a very low electronic conductivity, whereas  $\text{MgSc}_2\text{Se}_4$  is also a good electron conductor.

Doping  $\text{MgSc}_2\text{Se}_4$  by Ti and Ce leading to  $\text{Ti}^{4+}$  and  $\text{Ce}^{4+}$  impurities, respectively, has been considered a means to lower and neutralize the electronic conductivity.<sup>[22]</sup> Still, a high electron conductivity has been observed in these materials, which has been related to the presence of defects or phase deformation.<sup>[26,29]</sup> Furthermore, it has been shown that for chalcogenide spinels containing lanthanoids the Mg mobility increases with the size of the lanthanoids.<sup>[30]</sup>

Note that spinel structures including transition metal ions such as Ti, Mn, Fe, and Co exhibit magnetic properties due to the filling of the  $3d$  shell which cause significant distortions of the crystal lattice, namely, trigonal distortion, as shown later. Such trigonal distortions have hardly been considered in determining the transport properties of sulfide and selenide spinels yet. However, there is ample evidence for the existence of trigonal distortions in oxide spinels,<sup>[31–33]</sup> rendering their existence in chalcogenide spinels very likely. As the physical and chemical properties of these compounds strongly depend on the  $d$  electrons, it is important to understand the role of electrons in the ionic ordering, lattice distortion, and magnetic properties. Specifically, there are no convincing explanations with respect to the factors that determine the spatial distribution of the cations over the tetrahedral or octahedral sites and also with regard to the dependence of the activation barriers for migration on the doping level.<sup>[34,35]</sup> Studies on concerted migration<sup>[36]</sup> and the impact of the structural framework on the ionic conductivity<sup>[37]</sup> were conducted to analyze the factors determining the energy barriers for migration. However, there are still open questions regarding the cation ordering within the lattice and ion mobility in the various concentrations.

In this article we report first-principles electronic structure calculations addressing the Mg-ion mobility in  $\text{MgB}_2\text{X}_4$  spinel structures. As mentioned previously, such spinels have been considered as both electrode and solid electrolyte materials, depending on their electronic conductivity and insertion energy. Still, a high ion mobility is critical for the battery performance both in electrodes and in solid electrolytes. Although we particularly focus on the electronic properties determining ion migration in these materials, we mostly disregard here whether the considered spinels are better suited as electrodes or solid electrolytes, as we are convinced that the principles underlying low ion mobilities in these materials are independent from whether they are eventually used as electrodes or solid electrolytes. We find a strong dependence of the stability of the octahedral versus tetrahedral sites on the ion concentration, which we explain by an octahedral distortion and the corresponding changes in the lattice constants. Based on geometric considerations, we identify the ratio of distances in the octahedron and tetrahedron  $k_{64}$  as a descriptor for the stability of the cations within the octahedral and tetrahedral sites in the spinel lattice. In addition, we show that a purely ionic interaction picture is insufficient to capture the physics and chemistry behind the ionic migration and site preference. These insights also provide a framework for proposing promising spinel materials with high ion mobility based on fundamental material properties.

## 2. Computational Details

First-principles calculations are conducted in the framework of density-functional theory (DFT)<sup>[38,39]</sup> to determine the properties of  $\text{MgB}_2\text{X}_4$  ( $B = \text{Sc, Ti, V, Cr, Mn, Fe, Co, Ni, Y, Al}$  and  $X = \text{S, Se}$ ) spinels with regard to Mg migration. Exchange-correlation effects are approximated within the generalized gradient approximation (GGA) using the Perdew–Burke–Ernzerhof (PBE) functional.<sup>[40]</sup> The calculations are performed using the projector augmented wave (PAW)<sup>[41]</sup> method as implemented in the Vienna Ab-initio Simulation Package.<sup>[42–44]</sup> The nudged elastic band (NEB)<sup>[45]</sup> method is used to determine Mg-ion migration barriers. A  $2 \times 2 \times 2$  supercell of the primitive spinel cell is constructed for the NEB calculations, including 56 atoms. The total energy is evaluated with a  $2 \times 2 \times 2$  k-point mesh. A plane wave cutoff of 520 eV is chosen in the expansion of the wave functions, and total energies are converged within  $1 \times 10^{-5}$  eV per supercell. The NEB calculations have only been performed for spinel structures with transition metals with empty  $d$  orbitals. For these systems, the pure PBE approach is sufficient to yield reliable electronic and structural properties, except for the exact size of the band gap. Thus, we also avoid the well-known problems in obtaining converged NEB results when using GGA + U approaches or hybrid functionals. The electronic properties of spinels with transition metals that have partially filled  $d$  bands have been obtained with the Heyd–Scuseria–Ernzerhof HSE06 functional<sup>[46]</sup> to correctly account for the electron correlation. We also checked whether van der Waals interactions play a role, but we found no significant effects upon including van der Waals dispersion corrections, so we did not further consider them in our study.

Mg-ion migration in the chalcogenides has been studied in the low (one Mg vacancy per supercell) and high (one Mg atom inside the supercell) vacancy limit. The structures were fully relaxed until the forces on the atoms were converged within  $0.05 \text{ eV } \text{Å}^{-1}$ . The NEB calculations have been conducted with four distinct images between the tetrahedral and octahedral sites to evaluate the Mg-ion migration trajectory. To minimize the interaction between the migrating Mg ions across periodic boundaries, a distance of  $10 \text{ Å}$  between them is chosen.

The Mg intercalation energy  $E_{\text{inter}}$  in the spinel structure with respect to a metallic magnesium anode is given by

$$E_{\text{inter}}(\text{Mg}) = E(\text{Mg}_{x+y}\text{B}_2\text{X}_4) - (E(\text{Mg}_y\text{B}_2\text{X}_4) + xE(\text{Mg})) \quad (1)$$

where  $E(\text{Mg}_y\text{B}_2\text{X}_4)$  is the total energy of the spinel with a Mg concentration  $y$  in the unit cell, and  $E(\text{Mg})$  is the cohesive energy of Mg bulk in the metal phase. The corresponding open circuit voltage ( $V_{\text{OC}}$ ) is then given by

$$V_{\text{OC}} = -\frac{E_{\text{inter}}}{zF} \quad (2)$$

where  $F$  is the Faraday constant and  $z$  corresponds to the elementary charges that are transferred upon the discharging reaction with  $z = 2$  for MIBs. When  $E_{\text{inter}}$  is expressed in electronvolts,  $V_{\text{OC}}$  in volts is simply given by  $E_{\text{inter}}/2$  for MIBs.

### 3. Results and Discussion

Among the complex transition-metal (B) oxides and chalcogenides, spinel structures with the composition  $\text{Mg}^{2+}\text{B}_2^{3+}\text{X}_4^{2-}$  correspond to the most promising Mg-ion conductors.<sup>[29,47,48]</sup> The spinel structure shown in **Figure 1** consists of a face-centered cubic lattice of X anions ( $X = \text{O}, \text{S}, \text{Se}$ ) with two kinds of interstices between the sites of the fcc lattice: tetrahedral interstices  $\text{MgX}_4$  and octahedral interstices  $\text{BX}_6$ . The  $\text{BX}_6$  octahedra form a network of edge-sharing chains, while the Mg ions are located in the tetrahedrally vacant spaces of X ions, forming the  $\text{MgX}_4$  units. The B sublattice of the spinel structure is known as the pyrochlore lattice with strong geometrical frustration effects. The Mg sublattice forms a diamond lattice. As far as the electronic structures of the transition metal spinels are concerned, the  $d$  orbitals split into the high-lying doubly degenerate  $e_g$  and low-lying triply degenerate  $t_{2g}$  orbitals caused by the crystal field splitting of the regular  $\text{BX}_6$  octahedron.

Note that it is well known that spinel oxides tend to exhibit a strong Jahn–Teller distortion upon lithium insertion, which leads to a reduction of the crystal symmetry from cubic to tetragonal symmetry. For example, the lithiation of the  $\text{LiMn}_2\text{O}_4$  spinel to  $\text{Li}_{2.2}\text{Mn}_2\text{O}_4$  is accompanied by a tetragonal distortion characterized by a  $c/a$  ratio of  $c/a = 1.16$ .<sup>[49,50]</sup> On the other hand, increasing the average oxidation state of manganese in these lithium manganospinel from 3.5+ to 4+ suppresses the

Jahn–Teller distortion connected at the same time with a transition from antiferromagnetic to ferromagnetic behavior.<sup>[51]</sup> In our calculations of the sulfide and selenide spinels, we carefully looked for possible Jahn–Teller distortions, but could not detect any. We attribute this to the predominant ferromagnetic order of these spinels, which makes them much more conducting than oxides due to the enhanced  $p$ – $d$  hybridization. Note furthermore that spinel oxides are also prone to spin inversion and that sulfide spinels such as  $\text{MgIn}_2\text{S}_4$  have been shown to exhibit an inverted spinel structure.<sup>[52]</sup> However, to the best of our knowledge the number of sulfide and selenide spinels with an inverted structure is still limited. For example, it has been carefully verified that  $\text{MgSc}_2\text{Se}_4$  does not exhibit inversion.<sup>[26]</sup> We also attribute this to the higher conductivity of sulfide and selenide spinels associated with more delocalized electronic states, which suppresses high-spin states and thus strong ligand-field stabilization, which would favor spinel inversion.

However, spinel structures often exhibit a trigonal distortion of the octahedra that corresponds to a displacement of the X ions along the  $[111]$  direction and changes the  $O_h$  octahedral symmetry to a  $D_{3h}$  octahedral symmetry but keeps the overall octahedral shape unchanged (see **Figure 2a**).<sup>[53]</sup> The trigonal distortion can be characterized by a  $u$  anion parameter<sup>[54]</sup> that reflects the displacement of the X ions along the  $[111]$  direction in units of the lattice constant  $a$ . Sickafus et al.<sup>[54]</sup> showed that this parameter can be expressed through the effective radii  $r(\text{Mg})$  and  $r(\text{B})$  of the Mg and metal cations, respectively, according to

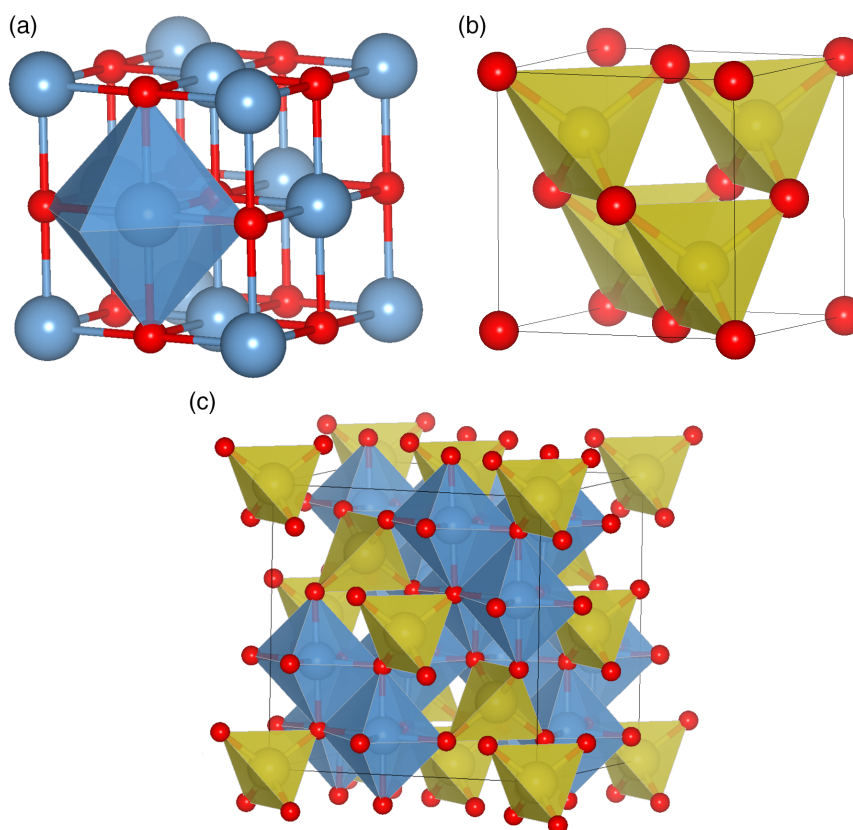


**Figure 1.** a) Rock-salt, b) zinc-blende, and c) spinel structure. The spinel lattice is an ordered mixture of the zinc-blende and rock-salt structure. The A species (yellow) of  $\text{AB}_2\text{X}_4$  occupy the tetrahedral sites, while the B species (blue) only occupy octahedral sites. The red spheres denote the oxide and chalcogenide anions such as  $\text{O}^{2-}$ ,  $\text{S}^{2-}$ , and  $\text{Se}^{2-}$ .

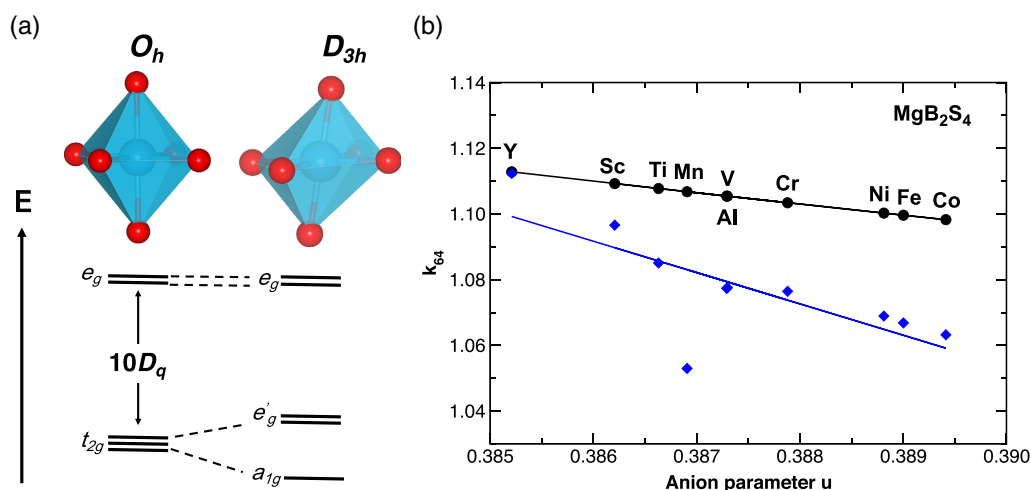


**Figure 2.** a) Illustration of the transition from an undistorted octahedron cage with a  $O_h$  octahedral symmetry to a trigonally distorted cage with a  $D_{3h}$  octahedral symmetry and the associated further crystal field splitting of the  $d$  states. b) Dependence of the ratio  $k_{64}$  on the anion parameter  $u$  characterizing the trigonal distortion for S spinels. The black dots denote the results for the original spinel structures with the Mg ion in a tetrahedral site and the octahedral vacancy being empty, and the black line corresponds to the analytical expression Equation (5). The blue diamonds are determined for the relaxed spinels with the octahedral site occupied by a Mg cation. The blue line is a linear regression of these results. Note that the results for V and Al lie on top of each other for both considered cases.

$$u = 0.3876 \left( \frac{r(B)}{r(Mg)} \right)^{-0.07054} \quad (3)$$

Interestingly, the effective radius of the X anions does not enter this expression, which means that the size of these anions obviously does not affect the trigonal distortions. For a value of  $u = \frac{3}{8}$ , an ideal spinel structure without any trigonal distortion results.  $u > \frac{3}{8}$  is associated with a trigonal distortion of the octahedra through which the tetrahedrons are enlarged at the expense of the octahedrons, whereas it is the other way around for  $u < \frac{3}{8}$ . The trigonal distortion of the octahedron further divides the threefold degenerate  $t_{2g}$  states into a lower  $a_{1g}$  state and a twofold degenerate  $e'_g$  state, as shown in Figure 2a. It should be noted that the representation of the  $a_{1g}$  state is  $\frac{1}{\sqrt{3}}(xy + yz + zx)$ , pointing toward the center of the B-lattice tetrahedron. The  $e'_g$  states are different from the doubly degenerate  $e_g$  states and they are perpendicular to the  $a_{1g}$  state. At low temperatures,<sup>[31]</sup> alternatively a tetragonal distortion often occurs, which splits the threefold degenerate  $t_{2g}$  states into a higher  $xy$  state and the twofold degenerate  $yz/zx$  lower states. The tetragonal distortion divides the doubly degenerate  $e_g$  states as well into  $x^2 - y^2$  and  $3z^2 - r^2$  states. Note, however, that the splitting of the  $t_{2g}$  states shown in Figure 2a is exaggerated; the calculated splitting is much smaller. Therefore we will in the following still refer to these two groups of states by calling them  $e_g$  and  $t_{2g}$  states for the sake of convenience.

Apart from the additional crystal field splitting, the trigonal distortions also modify the bonding distances, as mentioned in the previous paragraph. This can be quantified by explicitly looking at the Mg–X distances  $d(cn_4)$  and  $d(cn_6)$  in the tetrahedral and octahedral sites, respectively. In the original spinel structures with the Mg ion in a tetrahedral site and the octahedral

vacancy being empty, these distances can be expressed as a function of the anion parameter  $u$  as<sup>[54]</sup>

$$\begin{aligned} d(cn_4) &= (u - \frac{1}{4})a\sqrt{3} \\ d(cn_6) &= (2(u - \frac{3}{8})^2 + (u - \frac{1}{8})^2)^{1/2}a \end{aligned} \quad (4)$$

Using Equation (4), the ratio  $k_{64}$  between the bond lengths in the octahedral and the tetrahedral sites is given by

$$k_{64} = \frac{d(cn_6)}{d(cn_4)} = \frac{(2(u - \frac{3}{8})^2 + (u - \frac{1}{8})^2)^{1/2}a}{(u - \frac{1}{4})a\sqrt{3}} \stackrel{u=0.375}{=} \frac{2}{\sqrt{3}} \quad (5)$$

Here we indicated that in the perfect crystal with  $u = 3/8 = 0.375$  the ratio is  $k_{64} = 2/\sqrt{3} \approx 1.15$ , which means that in this structure the Mg–X bond length in the octahedral sites is 1.15 times larger than the tetrahedral bond length.

In Figure 2b, we have plotted the ratio  $k_{64}$  as a function of the anion parameter  $u$  for a number of ternary Mg spinels. The upper black circles correspond to the values for the Mg ion in a tetrahedral site and the octahedral vacancy being empty. It is obvious that  $k_{64}$  decreases approximately linearly with  $u$  in the small considered interval of  $u$  values which are larger than the value of 0.375 for the ideal structure; i.e., for all considered spinels the size of the tetrahedra is enlarged at the expense of the octahedron.

Furthermore, it is important to note that in the presence of the Mg ions in the octahedral vacancy,  $k_{64}$  is further reduced, as shown by the blue symbols in Figure 2b. Therefore, due to the explicit interaction of Mg cations with the surrounding chalcogenide anions, the size of the octahedrons further shrinks with respect to the tetrahedron. The dependence of  $k_{64}$  on  $u$  is in general still linear, but there are outliers. This is particularly obvious for MgMn<sub>2</sub>S<sub>4</sub>, where the presence of Mn apparently leads to a significant compression of the occupied octahedron. Interestingly enough, the size of the trigonal distortions is not



exactly ordered according to  $d$ -state occupation but rather according to decreasing crystal ionic radii as listed by Shannon,<sup>[55]</sup> suggesting that the change in these radii acts as one of the main driving forces for the trigonal distortions.

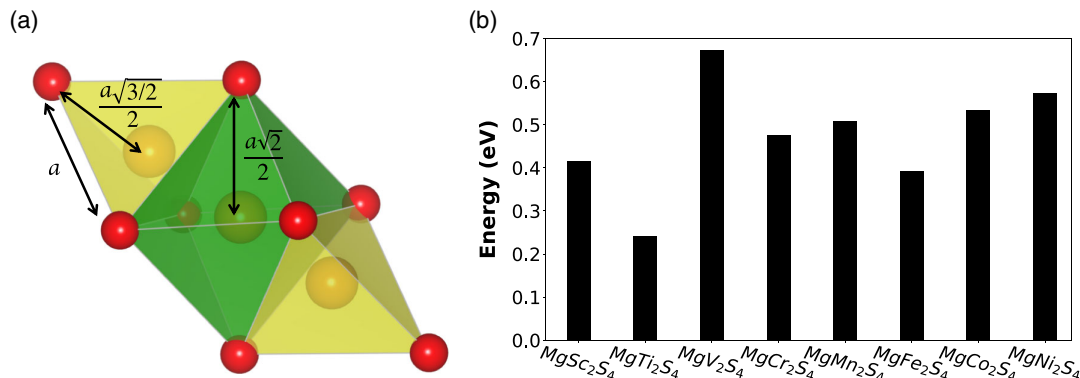
We now focus on the Mg mobility in the ternary spinel structures. The Mg-ion migration occurs between two tetrahedral sites via the migration across the face-sharing octahedral void, which is shown in **Figure 3a**. The transition state for the Mg migration is located in the triangular face between the octahedral and tetrahedral sites. The magnitude of the activation energy  $E_a$  is influenced by the anion species and the size of the triangle. Oxide cathode materials typically exhibit sluggish  $Mg^{2+}$  migration kinetics and also limited cycle life. One way to reduce the magnitude of the  $Mg^{2+}$  migration barriers is using the concept of hardness/softness of ions,<sup>[26,56]</sup> which can be related to the polarizability of the ions<sup>[57]</sup> or the covalency of the interaction.<sup>[58]</sup> Using “softer” anions than oxygen, namely, S, Se, or Te, leads to a weaker Coulombic attraction and a larger lattice constant, which also increases the distance between the guest  $Mg^{2+}$  and the host lattice, thus enhancing ion mobility. Note that in fact the degree of covalency can be quantified by the square of the difference in the electronegativities of the migration cation and the anion of the host lattice.<sup>[59]</sup> However, an increase in the ion mobility is typically associated with a reduction of energy density because low diffusion barriers are usually accompanied by small intercalation energies.

Figure 3b shows the calculated  $Mg^{2+}$  migration barriers of some selected sulfide spinels. All compounds represent Mg-ion migration energy smaller than 0.7 eV, confirming the relatively good  $Mg^{2+}$  conductivity in these spinel structures.  $MgTi_2S_4$  is identified as a suitable Mg-ion conductor; however, this compound is found to be unstable in the spinel structure and to exhibit electronic conductivity.<sup>[60]</sup> Sulfide spinels enhance the  $p$ - $d$  hybridization compared to oxides and tend to be more conducting. The various transition metal ions with  $d^1$ - $d^{10}$  configurations lead to magnetic structures that are caused by the strong Coulomb repulsion within the  $d$  orbitals.<sup>[61]</sup> In addition, smaller crystal ionic radii of the transition metals lead to decreased atomic distances and add more trigonal distortion to the system, as shown in Figure 2b. This obviously increases the Mg migration barriers. Hence, transition metals with occupied  $d$  orbitals in

general reduce the Mg-ion conductivity depending on the particular orbital character. Transition metal ions such as Sc with empty  $d$  orbitals, in contrast, lead to small migration barriers. In particular, the  $MgSc_2S_4$  spinel compound represents a balance between small  $Mg^{2+}$  migration energies and sufficient structural stability. Thus, in the following we will only focus on  $MgB_2X_4$  compounds with empty  $d$  orbitals which are characterized by high Mg-ion mobility according to our calculations. It is interesting to note that an analogous trend has been found in a recent computational study of Mg migration in lanthanoid chalcogenide spinels.<sup>[30]</sup> In these systems, apparently the height of the Mg migration barriers increases with higher  $f$ -state occupancy.

To elucidate the influence of the electronic structure on the properties of the spinels, we plotted in **Figure 4** the density of states (DOS) of  $MgB_2X_4$  spinels with  $B = Sc$  and  $Y$  and  $X = S$  and  $Se$  that can be realized experimentally.<sup>[62,63]</sup> Note that these spinel structures also exhibit trigonal distortions, but they are smaller than those for the spinels with later  $d$ -band metals, as shown in Figure 2b. In Sc and Y, the  $d$  orbitals are empty, which leads to unoccupied  $t_{2g}$  (green) and  $e_g$  (yellow) manifolds. In both compounds, with Sc and Y cations, respectively, the valence bands are dominated by S- and Se- $p$  bands, respectively, in the energy range from  $-4$  to  $0$  eV. For both systems, the DOS of the  $t_{2g}$  and  $e_g$  states are rather broad and overlap with each other. The main effect of replacing S ions by Se ions is a reduction of the bandgap by about  $0.5$  eV and a smaller ligand field splitting between antibonding  $e_g$  and nonbonding  $t_{2g}$  states. In the valence band shown in Figure 4,  $d$ -derived states appear, although Y and Sc in principle have no occupied  $d$  states in the conduction band. These states originate from the hybridization between the  $d$  states of the transition metal and the chalcogenide  $p$  bands,<sup>[64]</sup> but they do not dominate the behavior of the valence band.

Due to the absence of  $d$  valence states in Sc and Y, these elements are not easy to oxidize or to reduce upon intercalation. Hence, the chalcogenide anions need to be involved in the associated redox processes. In fact, this anion-based redox chemistry (anionic redox) has recently drawn quite some attention with respect to the increase in the energy density of Li-, Na- and Mg-ion batteries.<sup>[65-67]</sup> To elucidate this anionic redox, we performed a Bader charge analysis<sup>[68]</sup> and calculated charge density



**Figure 3.** a) Illustration of single-ion migration from the tetrahedral site to the octahedral void and then to the next tetrahedral site. The chalcogenide atoms such as S and Se are shown by the red spheres; the migrating Mg ions are presented by the spheres inside the tetrahedrons and the octahedron. b) Calculated Mg migration barriers for several transition metal ions in the sulfide spinels.

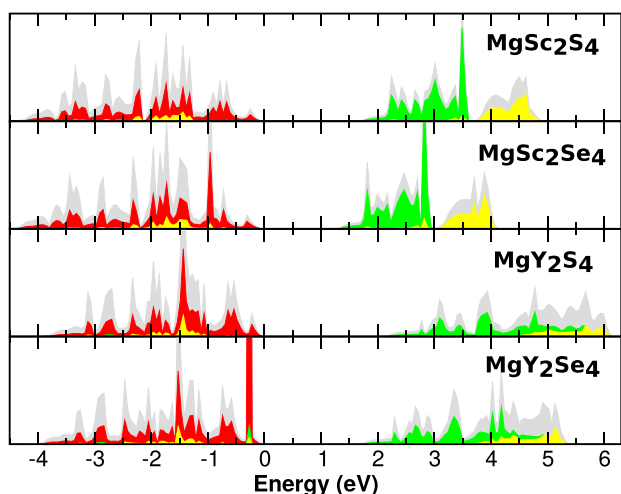


**Figure 4.** Density of states for  $\text{MgSc}_2\text{S}_4$ ,  $\text{MgSc}_2\text{Se}_4$ ,  $\text{MgY}_2\text{S}_4$ , and  $\text{MgY}_2\text{Se}_4$  from top to bottom. The total DOS is given in gray. The projected DOS are shown in red for S and Se, in green for  $t_{2g}$ , and in yellow for  $e_g$   $d$  orbitals. The energy zero is set to the top of the valence band.

differences<sup>[69]</sup> for  $\text{MgSc}_2\text{S}_4$ . Details of this charge analysis can be found in the Supporting Information. Specifically, we considered the insertion of Mg into an octahedral site of the host  $\text{Sc}_2\text{S}_4$  lattice at a low concentration resulting in a  $\text{Mg}_{0.125}\text{Sc}_2\text{S}_4$  structure. We find that this insertion leads to a reduction of the sulfur atoms reflected by a change of the S Bader charge from  $-0.86e$  to  $-1.08e$  (see Figure S2, Supporting Information), whereas Sc hardly participates in the reduction process. This confirms previous findings that the classical description of the redox process is no longer valid when the Fermi level becomes close to the S/Se- $p$  band.<sup>[65]</sup>

In fact, even for spinel transition metals containing a finite number of  $d$  electrons anionic redox can occur, as our calculations for  $\text{MgCr}_2\text{S}_4$  show. Upon Mg insertion into the  $\text{Cr}_2\text{S}_4$  host lattice at a high Mg concentration, the S atoms become reduced from a Bader charge of  $-1.02e$  to  $-1.30e$ , which is much stronger than the accompanying reduction of the Cr atoms. In contrast, in  $\text{MgCr}_2\text{O}_4$  both the Cr  $d$  and O  $p$  orbitals participate in a comparable fashion in the redox process according to our calculations (see the Supporting Information). This indicates that in sulfide and selenide spinels the anionic redox should be much more dominant than in oxide spinels, which can be traced back to the much lower electronegativity of the chalcogenides S and Se compared to oxygen.

**Table 1.** Mg–X, B–X, B–B, and Mg–Mg bond lengths in angstroms for spinel compounds. B and X denote transition metal (Sc, Y) and anion (S, Se), respectively. Calculated relative barrier energy  $E_a$ , intercalation energy  $E_{\text{inter}}^{\text{high}}$  ( $E_{\text{inter}}^{\text{low}}$ ) (Equation (1)) for high (low) Mg concentration in electronvolts, and corresponding open-circuit voltage  $V_{\text{OC}}^{\text{high}}$  ( $V_{\text{OC}}^{\text{low}}$ ) in volts. The volume changes with respect to the structure without Mg are indicated by  $\Delta V/V$

Compound	Mg–X [Å]	B–X [Å]	B–B [Å]	Mg–Mg [Å]	$E_a$ [eV]	$E_{\text{inter}}^{\text{high}}$ [eV]	$V_{\text{OC}}^{\text{high}}$ [V]	$E_{\text{inter}}^{\text{low}}$ [eV]	$V_{\text{OC}}^{\text{low}}$ [V]	$\Delta V/V$ [%]
$\text{MgSc}_2\text{S}_4$	2.464	2.593	3.784	4.634	0.415	–5.149	2.574	–5.165	2.582	–10
$\text{MgSc}_2\text{Se}_4$	2.587	2.725	3.974	4.868	0.375	–3.915	1.958	–4.114	2.057	–5
$\text{MgY}_2\text{S}_4$	2.510	2.740	3.949	4.836	0.360	–5.508	2.754	–5.561	2.780	+4.8
$\text{MgY}_2\text{Se}_4$	2.624	2.868	4.131	5.059	0.361	–4.329	2.165	–4.432	2.216	–2

Table 1 lists calculated properties of the considered spinel systems. These include structural properties of  $\text{Mg}(\text{Sc}/\text{Y})_2(\text{S}/\text{Se})_4$  spinels, the Mg migration barrier, the Mg intercalation energy, and the open-circuit voltage in the high and low Mg concentration limit, and the volume change upon Mg intercalation. Based on the calculations,  $\text{MgY}_2\text{Se}_4$  is a favorable candidate due to the combination of a small migration barrier, a sufficiently large open-circuit voltage, and a small volume change.  $\text{MgSc}_2\text{Se}_4$  and  $\text{MgY}_2\text{S}_4$  are also characterized by parameters that make them suitable as Mg-ion conductors. However, the performance of  $\text{MgY}_2\text{S}_4$  is deteriorated, despite a high open-circuit voltage  $V_{\text{OC}}$ , by an unfavorable volume expansion of almost 5% upon Mg-ion removal. At first sight, this volume expansion upon removal of some atoms is surprising. Therefore, we also considered the volume change  $\Delta V/V$  upon Mg-ion removal for a number of spinel oxides. Interestingly enough, we find a further enhanced tendency toward volume expansion in these oxides compared to the sulfides. Obviously, there is competition between volume reduction due to the removal of atoms and volume expansion as a consequence of the increased anion repulsion upon reducing the number of Mg cations, and this repulsion increases with the hardness of the anions.

To further assess the ion mobility in these spinel structures, the energies along the Mg migration paths for  $\text{MgSc}_2(\text{S}/\text{Se})_4$  and  $\text{MgY}_2(\text{S}/\text{Se})_4$  for high and low concentrations of Mg ions are plotted in Figure 5. Note that in the high Mg-ion concentration limit, there are seven Mg ions in the  $2 \times 2 \times 2$  supercell located in the tetrahedral sites, one of which is migrating, whereas in the low Mg-ion concentration limit, there is only one Mg ion in the supercell, which is also the migrating ion. The Mg-ion migration barriers of  $\text{MgY}_2\text{S}_4$  ( $\approx 360$  meV),  $\text{MgY}_2\text{Se}_4$  ( $\approx 361$  meV), and  $\text{MgSc}_2\text{Se}_4$  ( $\approx 375$  meV) in the high Mg concentration limit are rather small, leading to a high Mg mobility which is comparable to  $\text{Li}^+$  in fast Li conductors. This suggests that S and Se spinel structures together with Sc and Y cations can act as excellent Mg conductors. Furthermore, the bandgaps of about 1.5 eV for the selenides and of about 2 eV for the sulfides should lead to a relatively low electron conductivity. Therefore, in principle, these materials might as well be considered promising candidates for solid electrolytes in Mg-ion batteries because of their high Mg-ion mobility. However, experiments still found a high electron conductivity in these compounds,<sup>[22]</sup> probably due to the presence of defects or phase deformations,<sup>[26,29]</sup> hindering their use as solid electrolytes, but thus making them suitable as electrode materials with high ion mobility.

In the low-Mg-concentration limit, the Mg-ion migration barriers in the S and Se spinels are increased compared to the

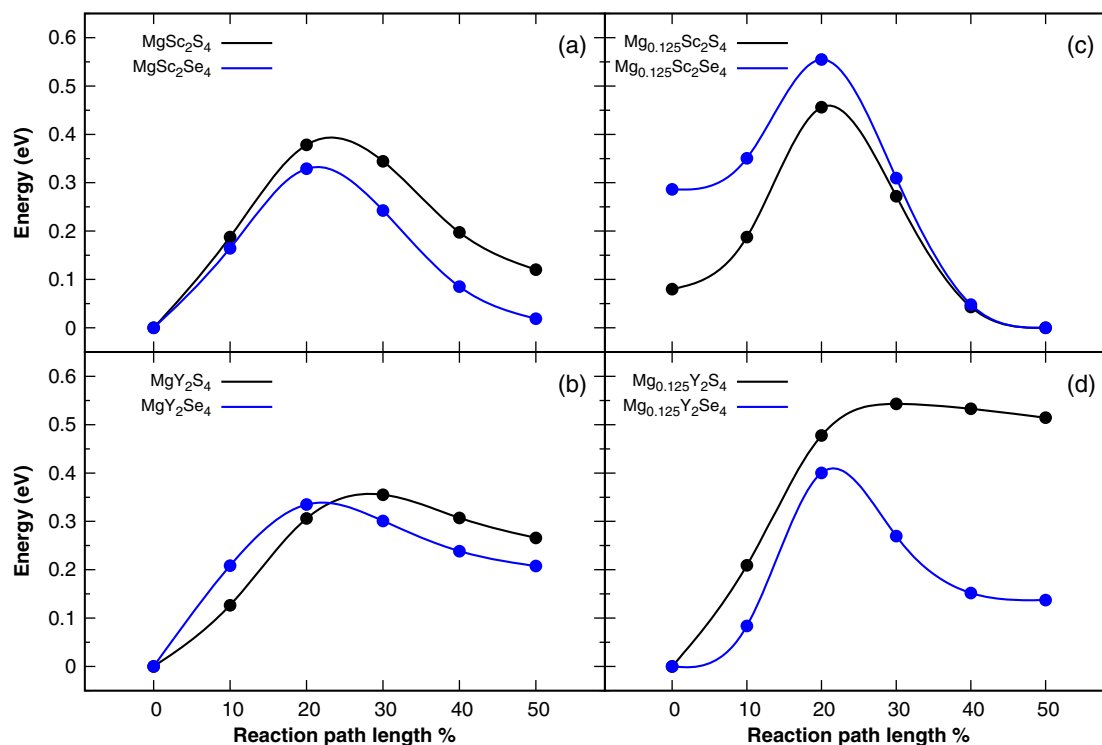


**Figure 5.** The  $\text{Mg}^{2+}$  migration energy barriers (in electronvolts) as a function of the reaction path coordinate derived from periodic DFT calculations combined with NEB for the single-ion migration from the tetrahedral site to the octahedral void corresponding to the S spinels (black) and the Se spinels (blue) for low and high concentrations of Mg ions. The low-concentration limit has been realized by considering just one migrating Mg atom within the  $2 \times 2 \times 2$  supercell, whereas in the high-concentration limit we consider one additional migrating Mg atom within a  $2 \times 2 \times 2$  supercell with a  $\text{Mg}_{0.875}\text{B}_2\text{X}_4$  stoichiometry. Note that the full migration path in principle includes the further migration from the octahedral to the tetrahedral site, but as the corresponding energies are symmetric with respect to the octahedral site, this part is omitted.

high-concentration limit, as shown in Figure 5. Furthermore, in  $\text{Mg}_{0.125}\text{Sc}_2(\text{S/Se})_4$  the Mg ion prefers the sixfold coordination of the octahedral site, whereas in  $\text{Mg}_{0.125}\text{Y}_2(\text{S/Se})_4$  the Mg-ion prefers the fourfold coordination of the tetrahedral site. Thus in the S and Se spinel structures together with Sc the most favorable site for the Mg ion changes from the octahedral to the tetrahedral site upon increasing the Mg concentration. This varying site preference, which is not the case for the Y cation, might be detrimental for the performance of the Sc-containing cathodes upon charge/discharge. In addition, the  $\text{MgY}_2(\text{S/Se})_4$  compounds exhibit smaller relative volume changes upon the addition of Mg atoms than the  $\text{MgSc}_2(\text{S/Se})_4$  compounds, which might be partly due to the fact Y has a larger crystal ionic radius than Sc.<sup>[55]</sup>

Up to now, we have concentrated on the electronic properties, structural parameters, and Mg migration paths. Of particular interest is that all  $\text{Mg}(\text{Sc/Y})_2(\text{S/Se})_4$  compounds favor the tetrahedral sites for the Mg ions. However, in the low-Mg-concentration limit, Mg ions prefer the octahedral site in the Sc spinels. To analyze this behavior, we will first concentrate on the high-Mg-concentration limit. Interestingly, according to our calculations  $\text{Mg}^{2+}$  tends to occupy the octahedral sites in the  $\text{MgMn}_2\text{S}_4$  spinel in the high-Mg-concentration limit. Here we will show that it is the competition between coordination and bond length induced by the trigonal distortion that governs

the Mg site preference in ternary spinel compounds  $\text{MgB}_2\text{X}_4$  ( $\text{B} = \text{Sc, Ti, V, Cr, Mn, Fe, Co, Ni, Y, Al}$  and  $\text{X} = \text{S, Se}$ ).

To see this, we focus on the ratio  $k_{64}$  between the Mg–X bond length in the occupied tetrahedral and octahedral sites, as shown for some ternary spinels by the blue symbols in Figure 2b. According to our calculations, for the  $\text{MgAl}_2\text{S}_4$  system characterized by a ratio of about  $k_{64} = 1.08$ , the octahedral and tetrahedral sites become energetically degenerate with regard to the Mg occupation, as shown in Figure 6a. This can be explained by a competition between bond length and coordination as a function of the ratio  $k_{64}$ . The octahedral site has the higher coordination than the tetrahedral site, but obviously in the ideal structure the elongation of the Mg–X bond length by 1.15 with respect to the tetrahedral site makes the octahedral site energetically still less favorable. However, for a decreasing ratio  $k_{64}$  the octahedral site becomes increasingly more stable with respect to the tetrahedral site. Note that the ratio  $k_{64} = 1.08$  is still larger than 1, but at this value the larger bond length is compensated for by the higher coordination of the octahedral site. For even smaller values of  $k_{64}$ , as for example in  $\text{MgMn}_2\text{S}_4$  with  $k_{64} = 1.05$ , the octahedral site is energetically more favorable, whereas for larger values of  $k_{64}$ , as in  $\text{MgSc}_2\text{S}_4$  with  $k_{64} = 1.10$ , the tetrahedral site becomes preferred (see Figure 6a).

A similar reasoning has recently been presented to understand the Mg tetrahedral site preference in lanthanoid

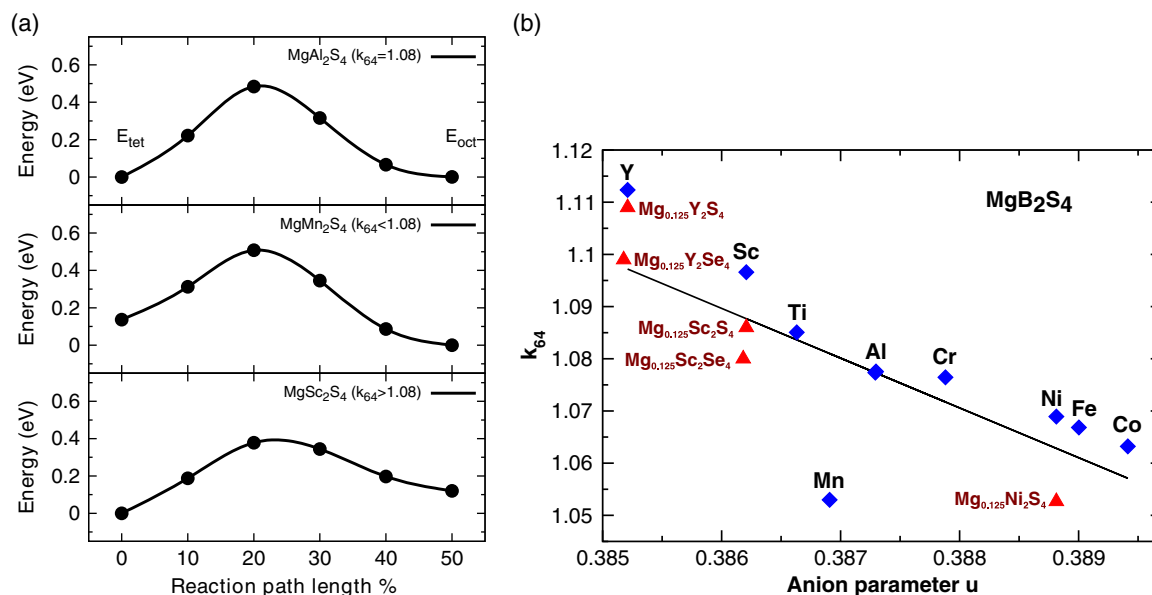


**Figure 6.** a) Mg-ion migration barriers for spinel compounds with different trigonal distortions characterized by  $k_{64}$ . b) The ratio  $k_{64}$  as a function of the anion parameter  $u$  for selected spinel compounds. Blue diamonds denote high-Mg-concentration compounds and red triangles low-Mg-concentration compounds. The black line represents a dividing line between Mg tetrahedral and octahedral site preference.

chalcogenide spinels,<sup>[30]</sup> based on the concept that the preference for coordination of a cation by an anion can be estimated by classic radii ratio rules. This argumentation about the competition between bond length and coordination implicitly assumes that the interaction is purely ionic between nonpolarizable atomic charges so that the ionic interaction is additive. Let us make a simple estimate about the stability of the tetrahedral Mg –  $X_4$  site versus the octahedral Mg –  $X_6$  site assuming that only the direct interaction between the  $\text{Mg}^{2+}$  cation and the neighbouring chalcogenide  $X^{2-}$  anions contributes to the interaction. For nonpolarizable, spherically symmetric, and nonoverlapping charges, the binding energies  $E(\text{Mg} - X_4)$  and  $E(\text{Mg} - X_6)$  in the tetrahedral and the octahedral arrangement, respectively, are given by

$$\begin{aligned} E(\text{Mg} - X_4) &= 4 \frac{Q_{\text{Mg}^{2+}} Q_{\text{X}^{2-}}}{d(\text{cn}_4)} = -\frac{16}{d(\text{cn}_4)} \\ E(\text{Mg} - X_6) &= 6 \frac{Q_{\text{Mg}^{2+}} Q_{\text{X}^{2-}}}{d(\text{cn}_6)} = -\frac{24}{d(\text{cn}_6)} \end{aligned} \quad (6)$$

where we have used cgs units for the sake of simplicity. For this purely ionic interaction the binding energies are the same, i.e.,  $E(\text{Mg} - X_4) = E(\text{Mg} - X_6)$ , for the ratio of

$$k_{64}^{\text{ionic eq.}} = \frac{d(\text{cn}_6)}{d(\text{cn}_4)} = 1.5 \quad (7)$$

First of all note that this ratio of 1.5 is much larger than the value of  $k_{64} = 1.08$  at which there is an equilibrium between the tetrahedral site and octahedral site in  $\text{MgAl}_2\text{S}_4$ . In addition, whether a spinel exhibits a tetrahedral or an octahedral site preference depends not only on the ratio  $k_{64}$ , but also on the anion parameter  $u$ . In Figure 6b, we again show the ratio  $k_{64}$  as a function of the anion parameter  $u$ , but now we also include some additional data points for the low Mg-concentration limit. In addition, we have inserted a dividing line given by

$k_{64}^{\text{div}} = 4.78(1 - 2u)$ . In spinels above this line, the migrating Mg ions prefer the tetrahedral site, whereas in those below this line, the octahedral site is more stable. Thus for larger values of  $u$ , the octahedral become more stable than the tetrahedral sites only for smaller values of the ratio  $k_{64}$ . In contrast, in the compounds nearby the dividing line, such as Ti, the occupation of both the tetrahedral and octahedral sites is energetically feasible, as also confirmed experimentally.<sup>[24]</sup>

To understand this trend, one should first note that according to Equation (4) both distances  $d(\text{cn}_4)$  and  $d(\text{cn}_6)$  become larger with increasing  $u$  in the parameter range that is considered here. However, for purely ionic interactions between nonpolarizable spherically symmetric ions, the competition in the energetic stability between two different structures does not depend on the absolute distances, only on the ratio of distances,<sup>[30,70–72]</sup> as reflected in the simple estimate in Equation (7). Consequently, these results can only be explained assuming that the interaction is not purely ionic and that it falls off stronger than  $1/d$  with distance  $d$ . Or, in other words, *covalent interactions contribute substantially to the stability of the Mg atoms in the voids*. Therefore, it follows that there is a simple criterion or descriptor that allows one to identify whether covalent interactions play a critical role in the relative stability of different structures: If the relative stability depends not only on the ratio of distances but also on the absolute value of these distances, then the interaction in these systems cannot be purely ionic.

The important role of covalent contributions in the interaction within the spinels is also reflected in the significant width in the DOS of the chalcogenide-derived states shown in Figure 4. For covalent and metallic interactions, the strengths of single bonds typically decrease with increasing coordination<sup>[15]</sup> based on bond-order conservation arguments, so the single bond becomes weaker for higher coordination. Furthermore, these interactions



scale with the overlap between atomic orbitals, which falls off exponentially for larger distances. Therefore, the ratio  $k_{64} = d(cn_6)/d(cn_4)$  needs to become smaller for absolute larger distances, i.e., for larger values of  $u$ , to make the octahedral more stable than the tetrahedral site.

Our findings provide a simple picture of the key parameter underlying Mg-ion site preferences in spinel structures. Similar to the Goldschmidt tolerance factor  $t$ ,<sup>[70]</sup> which is used to reflect the variance in the stability of perovskites based only on the ratio of the atomic radii of A, B, and X in  $ABX_3$ , we use a geometrical analysis to assess the relative stability of the  $Mg^{2+}$  sites in spinels. Our calculations and considerations of the structure of the spinel compounds clearly indicate that it is the ratio *together* with the absolute values of the Mg–X bond lengths in the octahedral and tetrahedral sites that determines the site preference and thus also the Mg mobility.

## 4. Conclusion

Based on periodic density functional theory calculations, we have studied Mg ion mobility in spinel chalcogenides, which are promising candidates for cathodes in MIBs. Overall, we find that trigonal distortions of the spinel structures play a critical role for both the Mg site preference and the Mg migration barriers. With respect to the transition metal used in the spinels, we find that an increasing  $d$ -band occupancy leads to smaller lattice constants and larger trigonal distortions, which both lead to larger migration barriers and thus decreasing diffusivities. In addition, according to our calculations anionic redox upon Mg insertion into the host lattice is more dominant in sulfide and selenide spinels than in oxide spinels. Therefore, we concentrated on spinel chalcogenide compounds with the early  $d$ -band metals Sc and Y together with the soft-ion chalcogenides S and Se.

Indeed, all these four considered spinels exhibit small diffusion barriers of about 400 meV and smaller. In addition, these materials allow open-circuit potentials with respect to metallic Mg of about 2.5 V for the sulfides and of about 2.0 V for the selenides. This makes them theoretically well suited as cathode materials for MIBs. In contrast, the low diffusion barriers together with the bandgap of about 1.5 eV for the selenides and of about 2 eV for the sulfides limiting their electronic conductivity suggests that these materials could also be used as solid electrolytes in MIBs because of their high Mg-ion mobility.

In many spinel structures studied so far, the tetrahedral sites exhibit a higher stability than the octahedral sites for Mg insertion. Interestingly, we find that in the Sc-based spinels this stability is reversed in the low-Mg-concentration limit. Our detailed analysis reveals that the varying site preference is a consequence of the competition between coordination and bond length induced by trigonal distortions and absolute changes in the bond distances demonstrating the important role of covalent contributions to the chemical interaction within the spinels. Thus, a purely electrostatic interaction is inadequate for capturing all factors influencing ion mobility and stability. In general, our results and the analysis based on electronic and geometric factors provide a conceptual framework to understand fast ion conductivity in spinel electrode materials, which will also be beneficial for the

understanding and improvement of ion mobility in other material classes.

## Supporting Information

Supporting Information is available from the Wiley Online Library or from the author.

## Acknowledgements

M.S. thanks Sung Sakong and Mohnish Pandey for fruitful discussions. The authors gratefully acknowledge financial support from the Cluster of Excellence POLiS (EXC-2154, project ID 390874152) of the Deutsche Forschungsgemeinschaft (DFG) and computer time provided by the state of Baden-Württemberg through bwHPC and the German Research Foundation (DFG) through grant no INST 40/575-1 FUGG (JUSTUS 2 cluster). This work contributes to the research performed at CELEST (Center for Electrochemical Energy Storage Ulm-Karlsruhe).

## Conflict of Interest

The authors declare no conflict of interest.

## Data Availability Statement

The data that support the findings of this study are available from the corresponding author upon reasonable request.

## Keywords

density functional theory, ion conductivity, magnesium batteries, ternary spinel chalcogenides

Received: June 1, 2021  
Revised: July 9, 2021  
Published online: August 4, 2021

- [1] J. Muldoon, C. B. Bucur, T. Gregory, *Chem. Rev.* **2014**, *114*, 11683.
- [2] P. Canepa, G. Sai Gautam, D. C. Hannah, R. Malik, M. Liu, K. G. Gallagher, K. A. Persson, G. Ceder, *Chem. Rev.* **2017**, *117*, 4287.
- [3] G. A. Elia, K. Marquardt, K. Hoepfner, S. Fantini, R. Lin, E. Knipping, W. Peters, J.-F. Drillet, S. Passerini, R. Hahn, *Adv. Mater.* **2016**, *28*, 7564.
- [4] M. Anji Reddy, M. Helen, A. Groß, M. Fichtner, H. Euchner, *ACS Energy Lett.* **2018**, *3*, 2851.
- [5] T. D. Gregory, R. J. Hoffman, R. C. Winterton, *J. Electrochem. Soc.* **1990**, *137*, 775.
- [6] D. Aurbach, Z. Lu, A. Schechter, Y. Gofer, H. Gizbar, R. Turgeman, Y. Cohen, M. Moshkovich, E. Levi, *Nature* **2000**, *407*, 724.
- [7] C. M. MacLaughlin, *ACS Energy Lett.* **2019**, *4*, 572.
- [8] R. Davidson, A. Verma, D. Santos, F. Hao, C. D. Fincher, D. Zhao, V. Attari, P. Schofield, J. Van Buskirk, A. Fraticelli-Cartagena, T. E. G. Alivio, R. Arroyave, K. Xie, M. Pharr, P. P. Mukherjee, S. Banerjee, *Mater. Horiz.* **2020**, *7*, 843.
- [9] N. Singh, T. S. Arthur, C. Ling, M. Matsui, F. Mizuno, *Chem. Commun.* **2013**, *49*, 149.
- [10] Z. Zhao-Karger, M. E. Gil Bardaji, O. Fuhr, M. Fichtner, *J. Mater. Chem. A* **2017**, *5*, 10815.

- [11] D. Aurbach, Y. Cohen, M. Moshkovich, *Electrochem. Solid-State Lett.* **2001**, 4, A113.
- [12] M. Matsui, *J. Power Sources* **2011**, 196, 7048.
- [13] Q. S. Zhao, J. L. Wang, *Electrochim. Acta* **2011**, 56, 6530.
- [14] M. Jäckle, A. Groß, *J. Chem. Phys.* **2014**, 141, 174710.
- [15] M. Jäckle, K. Helmbrecht, M. Smits, D. Stottmeister, A. Groß, *Energy Environ. Sci.* **2018**, 11, 3400.
- [16] E. Levi, Y. Gofer, D. Aurbach, *Chem. Mater.* **2010**, 22, 860.
- [17] Z. Zhao-Karger, R. Liu, W. Dai, Z. Li, T. Diemant, B. P. Vinayan, C. Bonatto Minella, X. Yu, A. Manthiram, R. J. Behm, M. Ruben, M. Fichtner, *ACS Energy Lett.* **2018**, 3, 2005.
- [18] M. M. Huie, D. C. Bock, E. S. Takeuchi, A. C. Marschilok, K. J. Takeuchi, *Coord. Chem. Rev.* **2015**, 287, 15.
- [19] M. Walter, K. V. Kravchyk, M. Ibáñez, M. V. Kovalenko, *Chem. Mater.* **2015**, 27, 7452.
- [20] C. B. Bucur, T. Gregory, A. G. Oliver, J. Muldoon, *J. Phys. Chem. Lett.* **2015**, 6, 3578.
- [21] J. Bitenc, K. Pirnat, T. Bančič, M. Gaberšček, B. Genorio, A. Randon-Vitanova, R. Dominko, *ChemSusChem* **2015**, 8, 4128.
- [22] L.-P. Wang, Z. Zhao-Karger, F. Klein, J. Chable, T. Braun, A. R. Schür, C.-R. Wang, Y.-G. Guo, M. Fichtner, *ChemSusChem* **2019**, 12, 2286.
- [23] T. Chen, G. Ceder, G. Sai Gautam, P. Canepa, *Front. Chem.* **2019**, 7, 24.
- [24] X. Sun, P. Bonnick, V. Duffort, M. Liu, Z. Rong, K. A. Persson, G. Ceder, L. F. Nazar, *Energy Environ. Sci.* **2016**, 9, 2273.
- [25] Z. Rong, R. Malik, P. Canepa, G. Sai Gautam, M. Liu, A. Jain, K. Persson, G. Ceder, *Chem. Mater.* **2015**, 27, 6016.
- [26] P. Canepa, S.-H. Bo, G. Sai Gautam, B. Key, W. D. Richards, T. Shi, Y. Tian, Y. Wang, J. Li, G. Ceder, *Nat. Commun.* **2017**, 8, 1759.
- [27] M. S. Islam, C. A. J. Fisher, *Chem. Soc. Rev.* **2014**, 43, 185.
- [28] A. Groß, *Top. Curr. Chem.* **2018**, 376, 17.
- [29] P. Canepa, G. Sai Gautam, D. Broberg, S.-H. Bo, G. Ceder, *Chem. Mater.* **2017**, 29, 9657.
- [30] J. Koettgen, C. J. Bartel, G. Ceder, *Chem. Commun.* **2020**, 56, 1952.
- [31] E. M. Wheeler, B. Lake, A. T. M. N. Islam, M. Reehuis, P. Steffens, T. Guidi, A. H. Hill, *Phys. Rev. B* **2010**, 82, 140406.
- [32] K. Matsuura, H. Sagayama, Y. Nii, N. D. Khanh, N. Abe, T. Arima, *Phys. Rev. B* **2015**, 92, 035133.
- [33] S. G. Menon, D. N. Hebbar, S. D. Kulkarni, K. Choudhari, C. Santhosh, *Mater. Res. Bull.* **2017**, 86, 63.
- [34] J. B. Goodenough, A. L. Loeb, *Phys. Rev.* **1955**, 98, 391.
- [35] J. B. Goodenough, *Energy Storage Mater.* **2015**, 1, 158.
- [36] X. He, Y. Zhu, Y. Mo, *Nat. Commun.* **2017**, 8, 15893.
- [37] Y. Wang, W. D. Richards, S. P. Ong, L. J. Miara, J. C. Kim, Y. Mo, G. Ceder, *Nat. Mater.* **2015**, 14, 1026.
- [38] P. Hohenberg, W. Kohn, *Phys. Rev.* **1964**, 136, B864.
- [39] W. Kohn, L. J. Sham, *Phys. Rev.* **1965**, 140, A1133.
- [40] J. P. Perdew, K. Burke, M. Ernzerhof, *Phys. Rev. Lett.* **1996**, 77, 3865.
- [41] P. E. Blöchl, *Phys. Rev. B* **1994**, 50, 17953.
- [42] G. Kresse, J. Hafner, *Phys. Rev. B* **1993**, 47, 558.
- [43] G. Kresse, J. Furthmüller, *Phys. Rev. B* **1996**, 54, 11169.
- [44] G. Kresse, D. Joubert, *Phys. Rev. B* **1999**, 59, 1758.
- [45] D. Sheppard, R. Terrell, G. Henkelman, *J. Chem. Phys.* **2008**, 128, 134106.
- [46] J. Heyd, G. E. Scuseria, M. Ernzerhof, *J. Chem. Phys.* **2003**, 118, 8207.
- [47] C. Kim, P. J. Phillips, B. Key, T. Yi, D. Nordlund, Y.-S. Yu, R. D. Bayliss, S.-D. Han, M. He, Z. Zhang, A. K. Burrell, R. F. Klie, J. Cabana, *Adv. Mater.* **2015**, 27, 3377.
- [48] J. Yin, A. B. Brady, E. S. Takeuchi, A. C. Marschilok, K. J. Takeuchi, *Chem. Commun.* **2017**, 53, 3665.
- [49] M. Thackeray, W. David, P. Bruce, J. Goodenough, *Mater. Res. Bull.* **1983**, 18, 461.
- [50] M. M. Thackeray, A. de Kock, M. H. Rossouw, D. Liles, R. Bittihn, D. Hoge, *J. Electrochem. Soc.* **1992**, 139, 363.
- [51] C. Masquelier, M. Tabuchi, K. Ado, R. Kanno, Y. Kobayashi, Y. Maki, O. Nakamura, J. B. Goodenough, *J. Solid State Chem.* **1996**, 123, 255.
- [52] G. Sai Gautam, P. Canepa, A. Urban, S.-H. Bo, G. Ceder, *Chem. Mater.* **2017**, 29, 7918.
- [53] S. K. Banerjee, W. O'Reilly, T. Gibb, N. Greenwood, *J. Phys. Chem. Solids* **1967**, 28, 1323.
- [54] K. E. Sickafus, J. M. Wills, N. W. Grimes, *J. Am. Ceram. Soc.* **1999**, 82, 3279.
- [55] R. D. Shannon, *Acta Crystallogr. Sect. A: Found. Crystallogr.* **1976**, 32, 751.
- [56] A. Grimaud, W. T. Hong, Y. Shao-Horn, J. M. Tarascon, *Nat. Mater.* **2016**, 15, 121.
- [57] J. Rungis, A. J. Mortlock, *Philos. Mag.* **1966**, 14, 821.
- [58] J. Rouxel, *Chem. Eur. J.* **1996**, 2, 1053.
- [59] M. Sotoudeh, A. Groß, Preprint, **2021**, <https://doi.org/10.21203/10.21203/rs.3.rs-309875/v2>.
- [60] A. Emly, A. Van der Ven, *Inorg. Chem.* **2015**, 54, 4394.
- [61] C. Lacroix, P. Mendels, F. Mila, *Introduction to Frustrated Magnetism: Materials, Experiments, Theory*, Springer Series in Solid-State Sciences, Springer, Berlin **2011**.
- [62] M. Patrie, L. Domange, J. Flahaut, C. R. Hebd. Seances Acad. Sci. **1964**, 258, 2585.
- [63] M. Guittard, C. Souleau, H. Farsam, C. R. Hebd. Seances Acad. Sci. **1964**, 259, 2487.
- [64] R. Asahi, Y. Taga, W. Mannstadt, A. J. Freeman, *Phys. Rev. B* **2000**, 61, 7459.
- [65] M. Ben Yahia, J. Vergnet, M. Saubanère, M.-L. Doublet, *Nat. Mater.* **2019**, 18, 496.
- [66] Z. Li, B. P. Vinayan, P. Jankowski, C. Njel, A. Roy, T. Vegge, J. Maibach, J. M. G. Lastra, M. Fichtner, Z. Zhao-Karger, *Angew. Chem. Int. Ed.* **2020**, 59, 11483.
- [67] N. Charles, Y. Yu, L. Giordano, R. Jung, F. Maglia, Y. Shao-Horn, *Chem. Mater.* **2020**, 32, 5502.
- [68] W. Tang, E. Sanville, G. Henkelman, *J. Phys. Condens. Matter* **2009**, 21, 084204.
- [69] M. Dillenz, M. Sotoudeh, H. Euchner, A. Groß, *Front. Energy Res.* **2020**, 8, 584654.
- [70] V. M. Goldschmidt, *Naturwissenschaften* **1926**, 14, 477.
- [71] V. M. Goldschmidt, *Trans. Faraday Soc.* **1929**, 25, 253.
- [72] V. Stevanović, M. d'Avezac, A. Zunger, *Phys. Rev. Lett.* **2010**, 105, 075501.